Laser and Particle Beams (2010), *28*, 45–52.

doi:10.1017/S0263034609990553

Influence of beam intensity profile on the aerodynamic particle size distributions generated by femtosecond laser ablation

A. MENÉNDEZ-MANJÓN,[1] S. BARCIKOWSKI,[1,2] G.A. SHAFEEV,[3] V.I. MAZHUKIN,[4] AND B.N. CHICHKOV[1,2]

[1]Laser Zentrum Hannover e.V., Hollerithallee 8, D-30419 Hannover, Germany
[2]Excellence Cluster REBIRTH, Hollerithallee 8, D-30419 Hannover, Germany
[3]General Physics Institute, 38 Vavilov street, 119991, Moscow, Russia
[4]Institute for Mathematical Modelling 4A Miusskaya Pl., 125047, Moscow, Russia

(RECEIVED 3 August 2009; ACCEPTED 29 October 2009)

Abstract

The dependence of nanoparticle size distributions on laser intensity profile was determined during infrared femtosecond laser ablation of silver targets in air. Laser parameters were adjusted to ablate at the same peak fluence with spatially homogeneous (flat-top) and inhomogeneous (Gaussian) intensity distributions formed by diffractive optical elements. Aerodynamic particle size was measured online by an electric low-pressure cascade impactor. Narrower size distributions were detected for the flat-top intensity profile in the fluence range from 0.6 to 4.4 J/cm^2, while the Gaussian beam produced broad and bimodal distributions. The aerodynamic number frequency of the primary nanoparticulate fraction (40 nm) was equal to the number frequency of the submicron agglomerate fraction (200 nm) at laser fluence of 1 J/cm^2. The Feret diameter of primary particles was 80 nm. Geometrical interpretation of the irradiated spots at the corresponding laser fluence regimes explains the formation of bimodal (submicron and nanoparticulate) size distribution in the case of Gaussian beams. The bimodality is attributed to different thermalization pathways during laser ablation.

Keywords: Airborne nanoparticles; Femtosecond laser ablation; Size distribution

1. INTRODUCTION

Ultrashort and short pulse lasers have found wide spread applications in various fields, since they offer high precision and reproducible machining because of the minimized thermal load and lower ablation thresholds compared to longer laser pulses (Chichkov *et al.*, 1996; Chaurasia *et al.*, 2008; Colgan *et al.*, 2008; Faenov *et al.*, 2008; Trtica *et al.*, 2009; Wang *et al.*, 2009). During laser machining, the formation of nanoparticles always occurs independent from the pulse duration or wavelength applied (Barcikowski *et al.*, 2007*a*, 2007*b*; Fazio *et al.*, 2009). For shorter pulse durations, nanoparticles are generated with higher efficiency (mass per energy) (Semerok *et al.*, 1999). The energy specific nanoparticle generation rate is one order of magnitude higher in the case of ultrashort, compared to nanosecond pulsed laser ablation in air (Bunte *et al.*, 2004). At the same pulse energy, femtosecond and picosecond pulses release similar share (>80%) of nanoparticles, quantified as airborne particles with aerodynamic size below 100 nm (Barcikowski *et al.*, 2008). In the same study, it has been shown that femtosecond laser ablation releases a significantly higher share of 7 nm sized nanoparticles during machining of metals (steel, brass) and ceramics (Zirconia). These nanoparticles may have the same chemical composition as the ablated material (iron-chromium-nickel alloy, yttria-doped zirconia). This indicates that nanoparticle formation happens in non-equilibrium state, as known from fundamental models of ultrafast laser ablation.

The ablated material ejected from the irradiated zone is made of ions, atoms, and nanoparticles with different atomization state depending on laser fluence. Fast imaging and emission spectroscopy experiments have proven that ablated matter splits in two components during the plume expansion: a fast component made up of atomic and ionic

Address correspondence and reprint requests to: Stephan Barcikowski, Laser Zentrum Hannover e.V., Hollerithallee 8, D-30419 Hannover, Germany. E-mail: s.barcikowski@lzh.de

species and a slow component consisting of clusters (Noël *et al.*, 2007).

Two different thermalization paths of the laser-excited electrons in the target occur depending on the absorbed laser fluence (Gamaly *et al.,* 2005*a*, 2005*b*, 2000). At low laser fluences optical absorption is responsible for superficial excitation of the target while at high laser fluence, thermal electron diffusion produces a deeper interaction. The thermodynamic evolution of the irradiated material and other external factors, for instance, the confinement of the plume, induce different ablation rates and ejected cluster morphology.

The majority of laser systems provide laser pulses with a Gaussian intensity distribution at the fundamental transversal mode:

$$F(r) = F_0 e^{\frac{-2r^2}{w_0^2}} \tag{1}$$

where F_0 is the peak fluence and w_0 is the beam radius ($1/e^2$). The fluence spatial distribution in the irradiated area may cause the coexistence of different ablation regimes at a single laser pulse. Given that the ablation mechanism depends on the laser fluence regimes, a uniform intensity profile should result in a better control on the ablation regimes (Eliezer *et al.*, 2004, 2005). Moreover, the presence of two populations of ablated material (fast and slow component) leads to broad size or even bimodal particle size distribution (Kabashin & Meunier, 2003), so that a uniform laser intensity distribution may produce monomodal and narrower size distributions. According to these aspects, we have studied the influence of the laser intensity distribution on the particle size distribution generated during femtosecond laser ablation of silver in air. (Fazio *et al.*, 2009; Latif *et al.*, 2009)

Beam shaping and homogenizing has been shown to improve the quality of laser machining during a variety of applications. Optical devices such as masks, refractive optics, mirrors, fiber bundles, and micro-optical elements are implemented for this purpose. However, the laser light is dispersed and absorbed in the optical set-up before reaching the target. With diffractive optical elements (DOE), phase front modification is induced by diffraction and not refraction. Hence, thinner devices are fabricated and for this reason, they exhibit enormous advantages for high power and ultrashort-pulsed laser technology (Momma *et al.*, 1998). We took advantage of these optical systems to compare the ablation of silver by a Gaussian and a flat-top intensity profile. The consequently generated nanoparticles were on-line captured and their aerodynamic diameter measured to study the changes on size distributions. Fumes and aerosols are characterized by their aerodynamic diameter (and not Feret diameter), as it has been shown to be the principal parameter for nanoparticles deposition mechanisms and rates of nanoparticles in filters or the respiratory system. For example, toxicological studies (International Commission on Radiological Protection, 1994) proved that particles with aerodynamic diameters of 20 nm are deposited in the alveolar region with an efficiency of 50% (Hinds, 1998). From this point of view, a correct control and characterization of airborne particles is interesting not only for the study of toxicological hazard but also for potential inhalative drug delivery (Borm & Kreyling, 2004).

2. EXPERIMENTAL SET-UP

Experiments were carried out with a Ti:Sapphire laser (Spectra Physics, Spitfire PRO, Mountain View, CA) delivering 120 fs pulses with a repetition rate of 5 kHz at a wavelength of 800 nm, and a maximal pulse energy of 300 μJ. The beam with 1.8 mm ($1/e^2$) radius was focused by an achromatic 100 mm focal length lens in order to obtain a Gaussian intensity profile. The flat-top profile was obtained with the implementation of the corresponding DOE (Silios Technologies, Peynier, France). Ablation took place inside a tubular chamber of 360 ml volume (constant volume flow rate of 10 l/min) in which the target was placed normal to the laser beam. An optical window on top allowed the entrance of the laser and full capture of the aerosol. An online-coulomb low-pressure cascade impactor (Dekati, ELPI, Tampere, Finland) connected to the chamber measured the particle size distributions at 1 Hz data acquisition rate in the aerodynamic diameter range from 7 nm to 10 μm. An example of the measurement results is presented in Figure 1. The particle number rate detected in each impactor stage is plotted as a function of time. The monotonous temporal trend of the results shows the constancy of the relative share of the particulate fractions during the ablation process. The different grey-shaded areas represent the total number of particles detected during 1 min (60 measurements). The fraction of microparticles is comparable low and is grouped to 1.2–6.2 μm fraction. The aerodynamic sized distribution ranges from 40–790 nm.

3. EXPERIMENTAL RESULTS

Particle generation experiments were carried out at the image plane of the DOE, determined with an optical microscope measuring the ablated patterns in a silicon wafer. In order to determine the dimensions of the beam, silicon was irradiated at different pulse energies with 50,000 pulses (50,000 on 1). From the ablated patterns (inset in Fig. 1), certain Gaussian intensity decay on the borders of the beam can be assumed. The ablated spot, D_{abl}, can hence be related to the real dimensions of the beam, L, as follows:

$$D_{abl}^2 = 2\left(\frac{L^2}{\pi}\ln(E_p) - \ln\left(\frac{L^2 F_{th}}{2}\right)\right), \tag{2}$$

as fluence is related to the pulse energy and beam side with:

$$F = \frac{E}{L^2}, \tag{3}$$

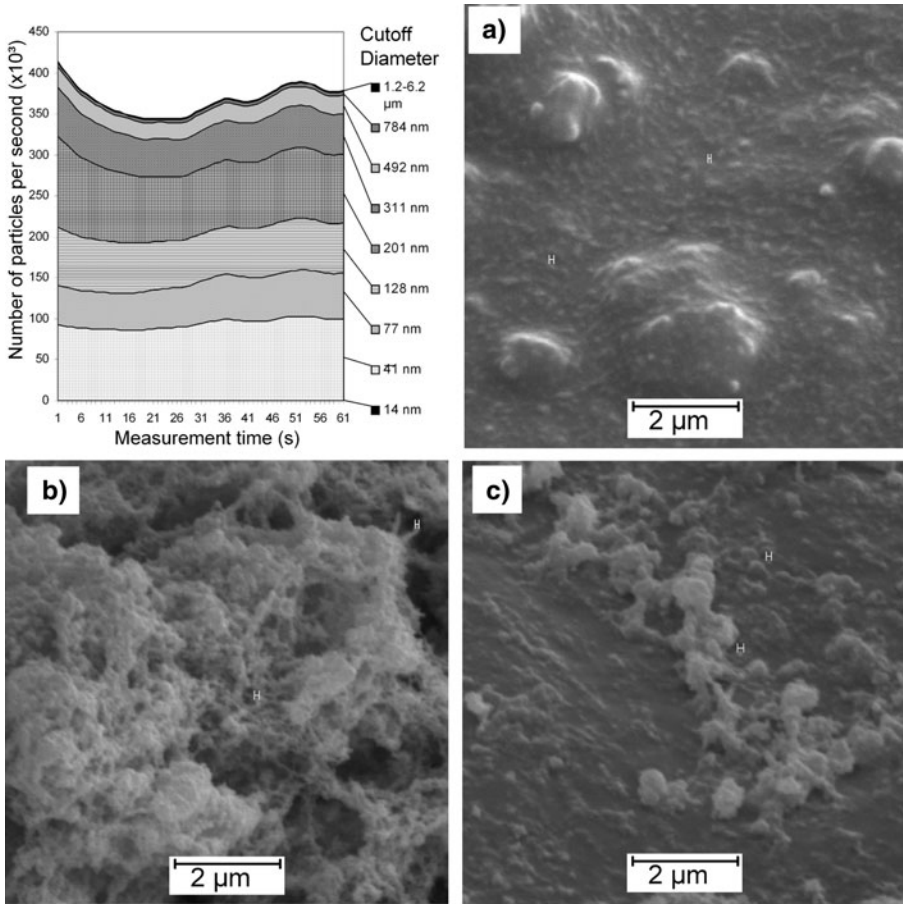

Fig. 1. Particle number rate at each stage of the cascade impactor and SEM micrographs of particles deposited on stages with cutoff diameter 40 nm (**a**), 201 nm (**b**), and 128 nm (**c**), generated by a laser ablation with Gaussian beam at 0.62 J/cm^2.

where E_p is the input pulse energy, F_{th} is the ablation fluence threshold. The resulting square side obtained from the semi-logarithmic fit is 57 ± 9 μm (Fig. 2).

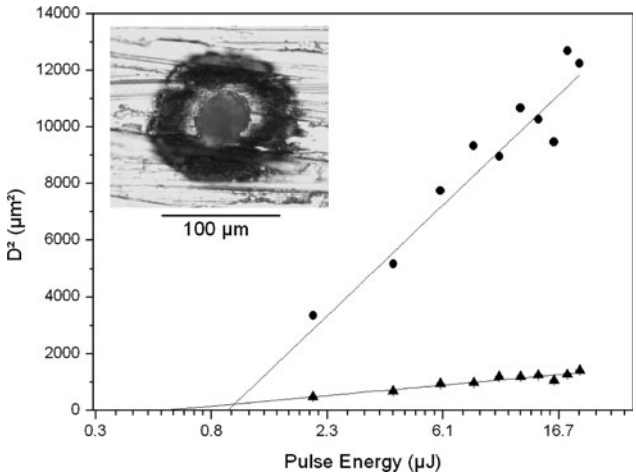

Fig. 2. Ablated spots of flat-top intensity profile in silicon at different pulse energies. The dashed line is the fit obtained with Eq. (2). Inset: typical ablated pattern.

Femtosecond laser ablation with Gaussian intensity distribution was made placing the target in the focal plane of the achromatic lens. The diffraction limited beam waist is 14 ± 1 μm. The pulse energy of the Gaussian beam necessary to have the same peak fluence as the flat-top profile is calculated based on the obtained beam dimensions. Of course, for tightly focused beams (Gaussian beam in our case), the pulse energy required to reach a determined peak fluence is much lower than for defocused beams (flat-top beam). The pulse energy for the Gaussian beam was varied form 2 to 13 μJ, while for the flat-top profile it was varied from 20 to 140 μJ.

Particle size distributions generated during femtosecond laser ablation of silver at 0.62, 1.25, 2.49, and 4.36 J/cm^2 and measured online are shown in Figure 3. In the fluence range from 0.62 to 3.74 J/cm^2 particle size distributions obtained by femtosecond laser ablation with Gaussian beam are bimodal. Two particle number frequency maxima appear at approximately 40 and 200 nm. This may be caused by the coexistence of two different ablation zones with cluster or particle densities. As fluence increases, the relative abundance of the small particles decreases, indicating that at higher peak fluence one of the two-ablation

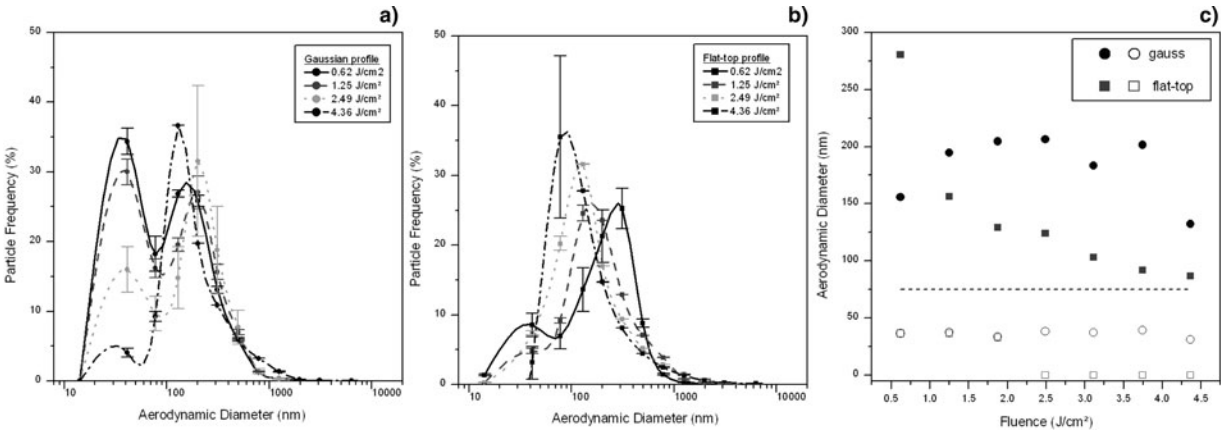

Fig. 3. Influence of the laser intensity profile on the particle size distributions generated by a Gaussian (**a**) and flat-top (**b**) profile at fluences 0.62, 1.25, 2.49, and 4.36 J/cm^2. (**c**) Mode values of the size distributions. Filled symbols represent the frequency maximum of big (submicron) particles and hollow symbols the frequency maximum of small (sub-100 nm) particle population.

mechanisms is dominant. At low fluences (0.64 and 1.25 J/cm^2) two-particle number frequency maxima are detected also in the case of the flat-top laser intensity profile, where at higher fluences >1.25 J/cm^2 the particle size distributions resulted monomodal (Fig. 3).

The bimodal particle distribution is consisting of submicron particles with aerodynamic diameter >75 nm and nanoparticles with diameter <75 nm. Laser fluence affects the number frequency of the respective particle population in the bimodal aerosol and the average particle diameter increases with the laser fluence applied. However, in the case of the Gaussian femtosecond laser beam the aerodynamic diameter of the particles remains almost constant for different laser fluences. In contrary, when a flat-top profile is used for femtosecond laser ablation of silver, the particle size of both populations is reduced as the fluence increases (Fig. 3c). As peak fluence applied for both beam profiles was the same, we attribute this effect to the pulse energy. An explanation could be that pulse energies above a certain threshold increase the particle concentration in the volume above the target. Independent from the intensity profile used for femtosecond laser ablation, an increase in the laser fluence causes a reduction in the population of small particles but an increase in the abundance of bigger particles (Fig. 3).

At about 1.2 J/cm^2, the number share of the two particle populations are equal in the case of Gaussian beam ablation. Assuming that particles size differences are originated in two ablation regions, at this laser fluence both mechanisms are balanced. Geometrically, the irradiated area on silver can be divided into two zones. The inner area, A_1, corresponds to fluences higher than a determined threshold, F_a, and the outer area, A_2, corresponds to fluences between the ablation threshold of silver, F_{th}, and F_a (Fig. 4).

These fluence thresholds were determined from the ablated patterns in silver (Fig. 5) with an ablation threshold F_{th} (from the outer diameter, D_{out}) of 0.031 J/cm^2 and F_a (from the inner diameter, D_{in}) of 0.19 J/cm^2. From Eq. (2), the relation between irradiated area and the corresponding threshold fluence can be determined as follows:

$$A_1 = \frac{\pi w_0^2}{2}\ln\left(\frac{F_0}{F_a}\right) \quad A_2 = \frac{\pi w_0^2}{2}\left\{\ln\left(\frac{F_a}{F_{th}}\right)\right\}. \tag{4}$$

These areas are supposed to be related to areas of two different thermalization mechanism of the target and consequently of two different nanoparticle populations formed subsequent to the thermalization. The dependence of the size of these two areas from the laser fluence is shown in Figure 7 for the experimentally determined parameters ($F_a = 0.19$ J/cm^2, $F_{th} = 0.03$ J/cm^2 and $w_0 = 14$ μm), predicting that at approximately 1 J/cm^2 both laser ablation mechanisms are equally dominant. This is in accordance to the experimental results in Figure 4a, where at about the same value (1.2 J/cm^2), the two nanoparticle populations were generated at equal number frequency.

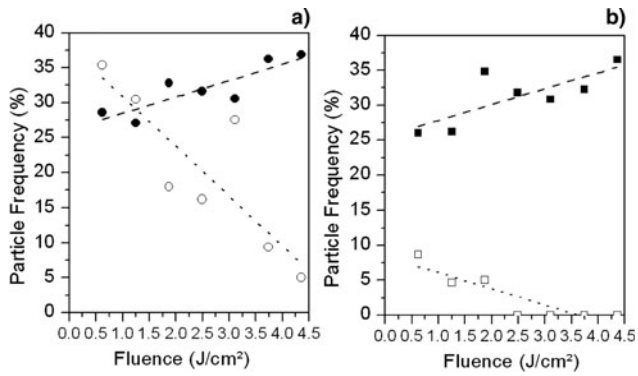

Fig. 4. Frequency of the peak maxima for aerodynamic particle size distribution generated by a Gaussian (**a**) and a flat-top (**b**) profile in the fluence range [0.6–4.4] J/cm^2. Filled symbols represent the particle frequency of peak maximum of particle >75 nm and hollow symbols the peak maximum of small particle population (<75 nm).

Table 1. *Physical constants of bulk silver*

Ω (kJ/g)	ρ (g/cm^3)	nk	M (g/mol)	A (Å)
2.36	10.49	5.29	107.8	4.09

The fluence threshold is related to the material density ρ, mass specific heat of vaporization Ω, and the laser-matter interaction depth inside the target l as follows:

$$F_{th} \approx l\Omega\rho. \tag{5}$$

With the material constants of bulk silver in Table 1 (Aschroft & Mermin, 1987; Palik, 1985) and the measured ablation thresholds from Figure 6, the laser matter, interaction depths for each range are 13 nm and 77 nm. The first corresponds to the skin depth of silver and the second to the thermal penetration depth of electrons. These values can be theoretically determined under certain approximations (Lehecka *et al.*, 2008):

$$l_{opt} = \frac{\lambda_0}{4\pi nk}; \quad l_{th} \approx a\sqrt{\frac{M_i}{3m_e}} \tag{6}$$

where nk, M, and a are the extinction coefficient, ion mass and interatomic distance of silver. The resulting interaction depths are 13 nm and 104 nm for the optical attenuation and the thermal diffusion, respectively, both confirming the experimental results.

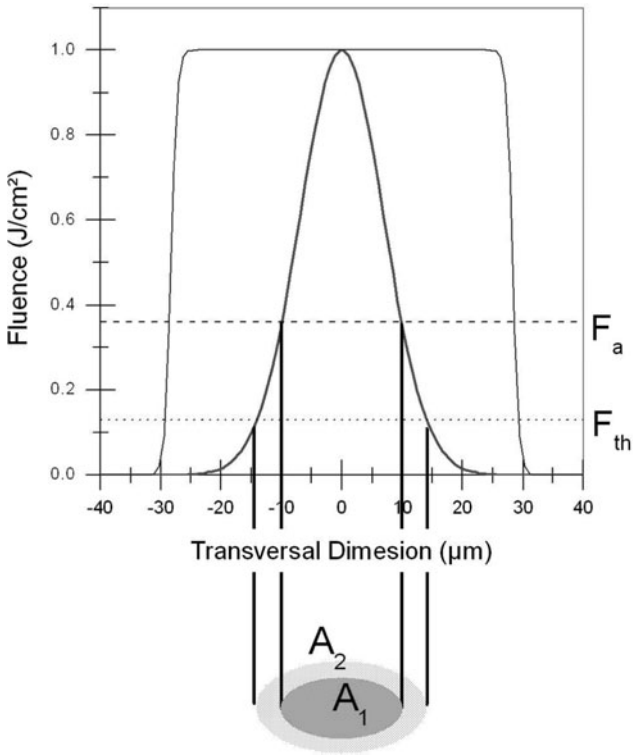

Fig. 5. Transversal laser fluence distribution for a Gaussian and flat-top profile. F_a and F_{th} represent the fluence thresholds for different ablation mechanism, and delimitate the irradiated areas with different fluence ranges.

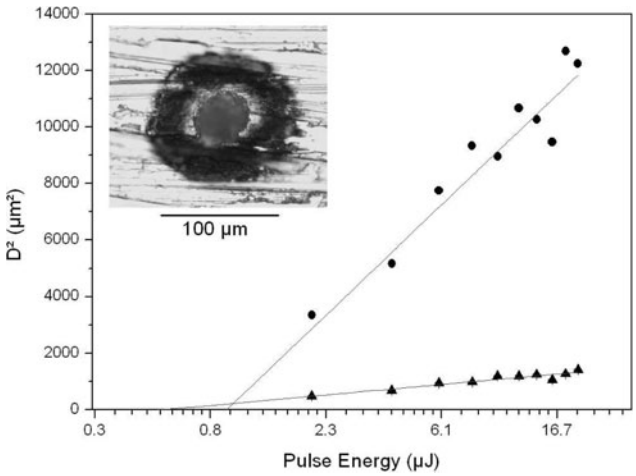

Fig. 6. Determination of ablation thresholds F_{th} and F_a: Square ablated diameters (inner, triangles; outer, circles) versus pulse energy. Inset: ablated spot on silver with 20 μJ.

The experiments and calculations confirm that the femtosecond laser generation of particles smaller than 75 nm is driven by soft ablation (low fluences) while the formation of particles bigger than 75 nm is based on hard ablation (high fluences). The normally distributed intensity in the laser beam implies the presence of those two ablation zones for one single pulse. Broad and even bimodal distributions are emitted from the target, where at the same peak fluence; homogeneously distributed laser intensities cause monomodal distributions.

From scanning electron microscope micrograph of the impacted aerosol presented in Figure 1, the Feret diameter of primary particles can be determined. On stage 2 (aerodynamic cut-off diameter 40 nm) we found mainly 80 nm particles but also big agglomerates (200 nm–1 μm). On stage 5 (aerodynamic cut-off diameter 201 nm) we found primary particles ranging from 90–230 nm and finally on stage 4, corresponding to an aerodynamic cut-off diameter of 128 nm, particles of Feret size of 80–120 nm are analyzed. It seems that particles collected by the cascade impactor consist of primary nanoparticles and agglomerates. The different agglomeration states are caused by different formation mechanism of airborne nanoparticles by femtosecond-laser ablation. Small primary nanoparticles agglomerate to bigger airborne nanoparticles. The agglomeration rate is related to the ablated matter density in the plume. Naturally, as at higher fluences more mass is ablated, the agglomeration rate increases. The formation of these agglomerates should take place in the strong ablation region (inner area in Fig. 6). The resulting aerodynamic diameters confirm this behavior. As shown in Figure 7, this region increases with laser fluence for a Gaussian beam. In analogy, the aerodynamic dynamic distribution varies with fluence. Primary particles $<$75 nm d_{Aero}

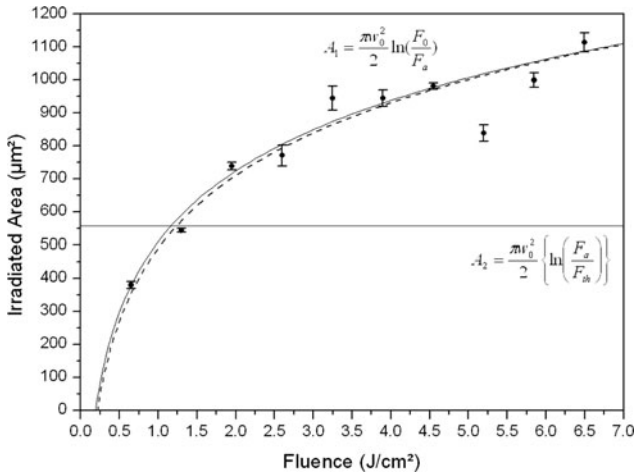

Fig. 7. Ablated area (circles) and calculated irradiated area (black line) for $F > F_a$ and calculated irradiated area for $F_{th} < F < F_a$ (horizontal line). The dashed line represents the best fit for the experimental data ($F_a = 0.21\,\mathrm{J/cm^2}$ $w_0 = 14.2\mu\mathrm{m}$).

(respectively < 150 nm d_{Feret}) tend to agglomerate and their population decreases, in favor of the >75 nm d_{Aero} (respectively < 150 d_{Feret}) population (Fig. 4).

Assuming a complete capture of the ablated material and a complete conversion of ablated mass into airborne particles (no redeposit was observed); the total volume of the particles detected in the impactor is proportional to the total ablated mass. The total ablated volume plotted against the laser fluence shows different tendencies for each beam profile (Fig. 8). In the case of Gaussian beam, low mass ablation rates are measured below a fluence of $3\,\mathrm{J/cm^2}$. This fluence is one order of magnitude bigger than the measured ablation threshold of silver ($0.19\,\mathrm{J/cm^2}$). At higher laser fluence, the ablated mass increases. In contrary, an almost linear increase in the ablated mass occurs for flat-top profile. This feature can be explained by the multiple reflections at the walls of the tapered ablated craters. As tapering is minimized for the holes machined by a flat-top profile, the incident radiation is normal to the target for each pulse. Therefore, less energy losses occur because of reflections. At sufficient high fluences the craters ablated by a Gaussian beam are so deep that the scattered laser is trapped inside the hole. Thus, the ablation is enhanced and results in deeper holes than the focal depth of the beam (Dahotre & Harimkar, 2007).

Laser processing of silver in a liquid environment results in different morphology of the surface. Indeed, laser ablation of silver targets in liquids may be considered as an alternative way for generation of silver nanoparticles that are free of any counter-ions and surface-active substances. The high purity of the resulting colloids and the possibility of one-step generation of nanoparticle-bioconjugates thrusts forward the laser-based synthesis technique (Petersen & Barcikowski, 2009; Petersen *et al.*, 2009). Presence of a liquid layer over an silver target alters the mechanism of melt removal. Namely, the molten layer that is formed on the target after the transfer of excitation from electrons to phonons is dispersed by recoil pressure of the liquid vapor adjacent to the target (Shafeev, 2008*b*). The molten layer is dispersed in the surrounding liquid as nanoparticles that have a bimodal size distribution in case of a Gaussian profile of a femtosecond laser beam (Shafeev *et al.*, 2004). At the threshold laser, fluence the molten layer on silver surface is modified due to the development of instability at the melt-vapor interface. Both the ablation rate and the rate of nanoparticles production drop, while the target becomes nano-textured as shown in Figure 9.

One can see that the size distribution of nanostructures is characterized by bimodal function centered on 20 and 50–60 nm, respectively. These nanostructures exhibit plasmon resonance typical of nano-sized silver around 400 nm. The ablated surface takes on the characteristic yellow coloration well visible at the angle of mirror reflection (Shafeev, 2008*a*). Note that the size of nanostructures in case of a

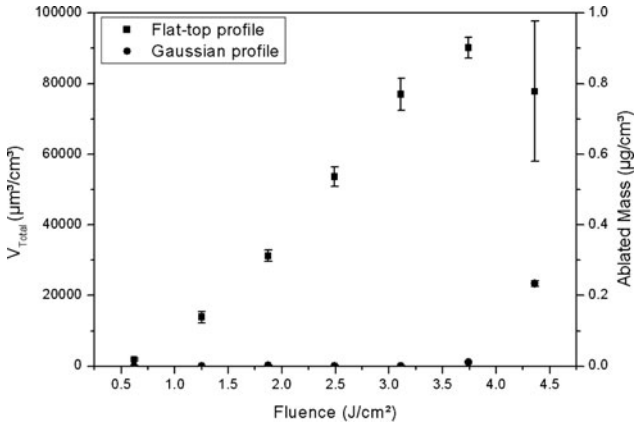

Fig. 8. Dependence of the total volume and mass ablated with flat-top and Gaussian intensity profile on the fluence.

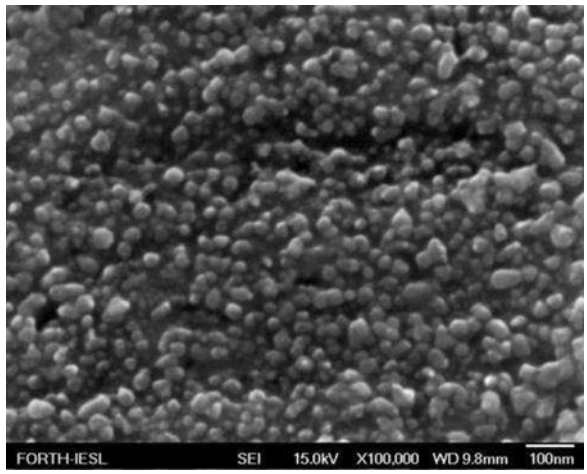

Fig. 9. Field emission scanning electron microscope view of the surface of an silver target subjected to ablation in water to radiation of a femtosecond laser at fluence of $4.5\,\mathrm{J/cm^2}$.

femtosecond laser pulses is much smaller than in case of a 350 ps laser exposure at the wavelength of 1.06 μm (Truong *et al.*, 2007). This difference, however, cannot be assigned to the difference in laser wavelength, since in case of silver target no wavelength-scaled periodic ripples are observed. Smaller size of nanostructures in case of a femtosecond laser exposure should be attributed to a thinner molten layer.

4. CONCLUSIONS

The influence of laser intensity profile on particle size distribution has been proven for femtosecond laser ablation of silver targets in air. Using homogeneous (flat-top) laser intensity profile, monomodal particle size distributions are generated, while Gaussian beam profile leads to bimodal particle size distributions. Bimodality of the lateral size of nanostructures on silver surface ablated under the layer of water apparently has similar origin. The customization of light field distribution allows a better control of the ablation process and aerodynamic nanoparticle size distribution. Particle transport in aerosol technology is characterized by the particle settling velocity, which is related to the aerodynamic diameter d_{Aero} measured by the cascade impactor. This property, (instead of the size d_{Feret} measured by scanning electron microscope) of airborne particles, has implications in inhalation toxicology and, at the same time, pharmacokinetic models and experimental design of inhalative particle drug delivery.

ACKNOWLEDGEMENT

The authors would like to thank the Deutsche Forschungsgemeinschaft for funding the nanoparticles research within the projects BA 3580/2-1 and CH-197/8-1.

REFERENCES

Ashcroft, N.W. & Mermin, N.D. (1987). *Solid State Physics*. New York: Harcourt College Publishers.

Barcikowski, S., Hahn, A. & Chichkov, B.N. (2007*a*). Nanoparticles as potential risk during femtosecond laser ablation. *J. Laser Appl.* **19**, 65–73.

Barcikowski, S., Hahn, A., Kabashin, A.V. & Chichkov, B.N. (2007*b*). Properties of nanoparticles generated during femtosecond laser machining in air and water. *Appl. Phys. A* **87**, 47–55.

Barcikowski, S., Walter, J., Hahn, A., Koch, J., Haloui, H., Herrmann, T. & Gatti, A. (2010). Picosecond and femtosecond laser machining may cause health risks related to nanoparticle emission of Laser Micro/Nanoeng (in press).

Borm, P.J.A. & Kreyling, W. (2004). Toxicological hazards of inhaled nanoparticles-potential implications for drug delivery. *J. Nanosci. Nanotech.* **4**, 521–531.

Bunte, J., Barcikowski, S., Puester, T., Burmester, T., Brose, M., Ludwig, T. (2004). Secondary hazards: Particle and X-ray emission. In *Femtosecond Technlolgy for Technical and Medical Applications*. pp. 309–321. Berlin: Springer.

Chaurasia, S., Munda, D.S., Ayyub, P., Kulkarni, N., Gupta, N.K. & Dhareshwar, L.J. (2008). Laser plasma interaction in copper nano-particle targets. *Laser Part. Beams* **26**, 473–478.

Chichkov, B.N., Momma, C., Nolte, S., Von Alvensleben, F. & Tunnermann, A. (1996). Femtosecond, picosecond and nanosecond laser ablation of solids. *Appl. Phys. A* **63**, 109–115.

Colgan, J., Abdallah, J., Faenov, A.Y., Pikuz, T.A., Skobelev, I.Y., Fortov, V.E., Fukuda, Y., Akahane, Y., Aoyama, M., Inoue, N. & Yamakawa, K. (2008). The role of hollow atoms in the spectra of an ultrashort-pulse-laser-driven Ar cluster target. *Laser Part. Beams* **26**, 83–93.

Dahotre, N.B. & Harimkar, S.P. (2007). Laser Drilling. In *Laser Fabrication and Micromachining of Materials* (Dahotre N.M. and Harimkar S.P., Ed). pp 97–137. New York: Springer.

Eliezer, S., Eliaz, N., Grossman, E., Fisher, D., Gouzman, I., Henis, Z., Pecker, S., Horovitz, Y., Fraenkel, M., Maman, S. & Lereah, Y. (2004). Synthesis of nanoparticles with femtosecond laser pulses. *Phys. Rev. B* **69**, 144119/1-6.

Eliezer, S., Eliaz, N., Grossman, E., Fisher, D., Gouzman, I., Henis, Z., Pecker, S., Horovitz, Y., Fraenkel, M., Maman, S., Ezersky, V. & Eliezer, D. (2005). Nanoparticles and nanotubes induced by femtosecond lasers. *Laser Part. Beams* **23**, 15–19.

Faenov, A.Y., Magunov, A.I., Pikuz, T.A., Skobelev, I.Y., Giulietti, D., Betti, S., Galimberti, M., Gamucci, A., Giulietti, A., Gizzi, L.A., Labate, L., Levato, T., Tomassini, P., Marques, J.R., Bourgeois, N., Dufrenoy, S.D., Ceccotti, T., Monot, P., Reau, F., Popescu, H., D'oliveira, P., Martin, P., Fukuda, Y., Boldarev, A.S., Gasilov, S.V. & Gasilov, V.A. (2008). Non-adiabatic cluster expansion after ultrashort laser interaction. *Laser Part. Beams* **26**, 69–81.

Fazio, E., Neri, F., Ossi, P.M., Santo, N. & Trusso, S. (2009). Ag nanocluster synthesis by laser ablation in Ar atmosphere: A plume dynamics analysis. *Laser Part. Beams* **27**, 281–90.

Gamaly, E.G., Luther-Davies, B., Kolev, V.Z., Madsen, N.R., Duering, M. & Rode, A.V. (2005*a*). Ablation of metals with picosecond laser pulses: Evidence of long-lived non-equilibrium surface states. *Laser Part. Beams* **23**, 167–176

Gamaly, E.G., Madsen, N.R., Duering, M., Rode, A.V., Kolev, V.Z. & Luther-Davis, B. (2005*b*). Ablation of metals with picosecond laser pulses: Evidence of long-lived nonequilibrium conditions at the surface. *Phys. Rev. B* **71**, 6310–6315.

Gamaly, E.G., Rode, A.V. & Luther-Davies, B. (2000). Formation of diamond-like carbon films and carbon foam by ultrafast laser ablation. *Laser Part. Beams* **18**, 245–254.

Hinds, W.C. (1998). *Aerosol Technology – Properties, Behavior, and Measurement of Airborne Particles*. New York: Wiley-VCH.

International Commission on Radiological Protection. (1994). *Human Respiratory Tract Model for Radiological Protection*. New York: Pergamon.

Kabashin, A.V. & Meunier, M. (2003). Synthesis of colloidal nanoparticles during femtosecond laser ablation of gold in water. *J. Appl. Phys.* **94**, 7941–7943.

Latif, A., Anwar, N.S., Aleem, M.A., Rafique, M.S. & Khaleeq-Ur-Rahman, M. (2009). Influence of number of laser shots on laser induced microstructures on Ag and Cu targets. *Laser Part. Beams* **27**, 129–136.

Lehecka, T., Mostovych, A. & Thomas, J. (2008). Long duration light emission from femtosecond laser–target interactions. *Appl Phys A* **92**, 727–741.

Momma, C., Nolte, S., Kamlage, G., Von Alvensleben, F. & Tünnermann, A. (1998). Beam delivery of femtosecond laser radiation by diffractive optical elements. *Appl. Phys. A* **67**, 517–520.

Noël, S., Hermann, J. & Itina, T. (2007). Investigation of nanoparticle generation during femtosecond laser ablation of metals. *Appl. Surf. Sci.* **253**, 6310–6315.

Palik, E.D. (1985). *Handbook of Optical Constants of Solids*. New York: Academic Press.

Petersen, S. & Barcikowski, S. (2009). In-situ bioconjugation - Single step approach to tailored nanoparticle-bioconjugates by ultrashort pulsed laser ablation. *Adv. Funct. Mater.* **19**, 1–6.

Petersen, S., Jakobi, J. & Barcikowski, B. (2009). In-situ bioconjugation of nanoparticles—Novel laser based approach to pure nanoparticle-conjugates. *Appl. Surf. Sci.* **255**, 5435–5438.

Semerok, A., Chaléard, C., Detalle, V., Lacour, J.L., Mauchien, P., Meynadier, P., Nouvellon, C., Sallé, B., Palianov, P., Perdrix, M. & Petite, G. (1999). Experimental investigations of laser ablation efficiency of pure metals with femto, pico and nanosecond pulses. *Appl. Surf. Sci.* 138–**139**, 311–314.

Shafeev, G.A. (2008*a*). Formation of nanoparticles under laser ablation of solids in liquids. In *Nanoparticles: New Research* (Lombardi S.L., Ed.), pp. 1–37. New York: Nova Science Publishers, Inc.

Shafeev, G.A. (2008*b*). Laser-based formation of nanoparticles. In *Lasers in Chemistry* (Lackner M., Ed.), Vol. 2, pp. 713–741. Weinheim, Germany: Wiley VCH.

Shafeev, G.A., Freysz, E. & Bozon-Verduraz, F. (2004). Self-influence of a femtosecond laser beam upon ablation of Ag in liquids. *Appl. Phys. A* **78**, 307–309.

Trtica, M.S., Radak, B.B., Gakovic, B.M., Milovanovic, D.S., Batani, D. & Desai, T. (2009). Surface modifications of Ti6A14V by a picosecond Nd:YAG laser. *Laser Part. Beams* **27**, 85–90.

Truong, S.L., Levi, G., Bozon-Verduraz, F., Petrovskaya, A.V., Simakin, A.V. & Shafeev, G.A. (2007). Generation of nanospikes via laser ablation of metals in liquid environment and their activity in surface-enhanced Raman scattering of organic molecules. *Appl. Surf. Sci.* **254**, 1236–1239.

Wang, Z., Zheng, H. & Zhou, W. (2009). Ultrashort laser subsurface micromachining of three-dimensional microfluidic structures inside photosensitive glass. *Laser Part. Beams* **27**, 521–528.